Plasma treatment causes structural modifications in lysozyme, and increases cytotoxicity towards cancer cells

Pankaj Attri[1,2,3]*, Nagendra Kumar Kaushik[4], Neha Kaushik[5], Dietmar Hammerschmid[6], Angela Privat-Maldonado[3], Joey De Backer[6], Masaharu Shiratani[1,2], Eun Ha Choi[4] and Annemie Bogaerts[3]

[1] Center of Plasma Nano-interface Engineering, Kyushu University, Fukuoka 819-0395, Japan
[2] Graduate school of Information Science and Electrical Engineering, Kyushu University, Fukuoka 819-0395, Japan
[3] Research group PLASMANT, Department of Chemistry, University of Antwerp, Antwerp, Belgium
[4] Department of Electrical and Biological Physics, Kwangwoon University, Seoul 01897, Korea
[5] Department of Biotechnology, College of Engineering, University of Suwon, Hwaseong, 18323, Korea
[6] Research Group PPES, Department of Biomedical Sciences, University of Antwerp, Universiteitsplein 1, Antwerp, Belgium

Bacterial and mammalian proteins, such as lysozyme, are gaining increasing interest as anticancer drugs. This study aims to modify the lysozyme structure using cold atmospheric plasma to boost its cancer cell killing effect. We investigated the structure at acidic and neutral pH using various experimental techniques (circular dichroism, fluorescence, and mass spectrometry) and molecular dynamics simulations. The controlled structural modification of lysozyme at neutral pH enhances its activity, while the activity was lost at acidic pH at the same treatment conditions. Indeed, a larger number of amino acids were oxidized at acidic pH after plasma treatment, which results in a greater distortion of the lysozyme structure, whereas only limited structural changes were observed in lysozyme after plasma treatment at neutral pH. We found that the plasma-treated lysozyme significantly induced apoptosis to the cancer cells. Our results reveal that plasma-treated lysozyme could have potential as a new cancer cell killing drug.

1. Introduction

The dynamic nature of cancer is one of the major problems for its treatment, as it can lead to drug resistance, causing the need for higher treatment doses, which can result in negative side effects in patients [1]. In the last few decades, experimental studies and clinical trials have aimed to assess alternative anti-tumor therapeutics, among others based on bacterial and animal products [2–4]. This is the case for lysozyme (animal and human) and porcine pancreatic enzyme extracts (PPE), which have been studied as potential cancer treatments [5–7]. Lysozyme is known to hydrolyze specific peptidoglycan linkages in the cell wall of bacteria, making it a natural antibacterial product. Lysozyme is produced in the body as a non-specific defense mechanism associated with the monocyte–macrophage system [8]. Interestingly, it has also shown potential as anticancer agent, as it can inhibit tumor formation and growth, and improve the efficiency of chemotherapeutic treatments [6,7]. Lysozyme is one of the main secretory products of macrophages and it is an essential mediator for anti-tumour activities [9–11]. It was reported that lysozyme plays a pivotal role in the human innate immune system [12]. Lysozyme inhibits interleukin-2-activated human peripheral blood lymphocytes [13] and could modify glycoprotein receptors in normal and neoplastic cells [14].

Lysozyme expression was found in gastric tumors and gastric Paneth cells [15–17], which suggests it is evoked as part of the defense mechanism against malignant cells [18]. Lysozyme inhibited the growth of human gastric cell lines like MGC803, MKN28, and MKN45, while it was not toxic towards normal human lung fibroblasts [19]. Lysozyme treatment promoted the immunoglobulin production by HB4C5 cells (human-human hybridoma line) and human peripheral blood lymphocytes [20,21]. Zheng et al. functionalized lysozyme on bioactive glass nanoparticles and showed that specific cytotoxicity was achieved only on cancer but not normal cells [6], indicating a possible selectivity towards cancer cells. Similarly, Mahnta et al. synthesized a self-assembled nanostructured lysozyme that exhibited anticancer activity against breast cancer cells (MCF-7) but was not toxic to normal cells [22]. So far, lysozyme has successfully demonstrated anticancer activity [20–22]. Still, there is significant potential to enhance the activity of lysozyme as cancer cell killing drug.

It is known that the enzymatic activity of proteins can be improved by modifying their structure using chemical and physical methods [23–25]. Atmospheric pressure plasma, a partially ionized gas that delivers a variety of reactive oxygen and nitrogen species (RONS), has proven to effectively modify the structure and function of several proteins. Some examples include the heme degradation of horseradish peroxidase [26], structural modification of α-chymotrypsin [27], NADPH oxidase activator (Noxa 1) [28], myoglobin [29,30], hemoglobin [31], MTH1880 [32], and bacteriorhodopsin [33]. In addition, plasma treatment has been shown to induce a modest increase in the activity of lipase and α-amylase [34,35]. In our previous research we evaluated the effect of two different plasma sources, i.e., a dielectric barrier discharge (DBD) and an atmospheric pressure plasma jet (APPJ) operating in N_2 and air, on the lysozyme lytic activity, and we observed that the air-DBD causes a less pronounced drop in lytic activity than a DBD operating in N_2 and the APPJ plasma [36]. In the present study, we are interesting to study in more detail whether plasma, and more specifically this air-DBD modified lysozyme, can cause cytotoxic effect on cancer cells, as this would allow the use of lower (non-toxic) concentrations of lysozyme to kill cancer cells.

This study aims to determine the structural modifications induced by plasma on lysozyme and assess its cytotoxicity. For this purpose, we have performed functional experiments and molecular dynamics simulations to identify the structural changes in lysozyme after plasma treatment. Overall, our experimental and computational studies suggest that modification at Trp and Tyr residues of lysozyme after plasma treatment enhances its activity, which opens a new avenue for the design of novel therapeutic approaches against cancer.

2. Materials and Methods

2.1. Materials

Lysozyme and other chemicals were supplied by Sigma-Aldrich Chemical Co. (USA). All chemicals and reagents were used without further purification.

2.2. Pulsed DBD plasma device

The pulsed DBD plasma source was developed by Plasma Bioscience Research Center, Korea, and details are described in our previous article [28]. Briefly, the DBD plasma

source was fabricated in coplanar configuration by using silver electrodes of width = 100 µm and thickness = 5 µm above a circular glass substrate (SiO_2). The diameter and thickness of the glass substrate were 35 mm and 1.8 mm, respectively. The spacing between adjacent silver electrodes on each plane was fixed at 2 mm. The V_{rms} was 1.17 kV, and I_{rms} was 16 mA. The discharge voltage was 1.08 kV, and the applied power was 3.88 J/s. The plasma on-time was 25 ms, and the off-time was 150 ms.

2.3. Plasma treatment of lysozyme solution for circular dichroism, fluorescence, and mass spectrometry analysis

A lysozyme solution at 0.2 mg/mL was used for secondary structure analysis by circular dichroism (CD). For the tertiary structure analysis by fluorescence spectroscopy, 0.5 mg/mL lysozyme solution was used, while for mass spectrometry (MS), 0.002 mg/mL was used. All lysozyme solutions were prepared in 10 mM phosphate buffer at pH 2 and 7. For plasma treatment, 1 mL solution was treated with the DBD device for 5, 10 and 20 min in a 6-well plate (Greiner) at a distance of 5 mm.

2.4. Circular dichroism (CD) spectroscopy

CD spectra of native and plasma-treated lysozyme were measured using JASCO J-815 spectropolarimeter (Jasco, Tokyo, Japan). The 0.2 mg/mL lysozyme solutions were pre-equilibrated at 25 °C for 15 min. The secondary structure of lysozyme was monitored using a 1 mm path length cuvette. Each spectrum was taken as the average of six spectra. Each sample spectrum was obtained by subtracting the blank (without lysozyme).

2.5. Temperature stability studies

Preliminary thermodynamic stability studies were performed by temperature-controlled J-815 spectrophotometry (Jasco, Japan) equipped with a Peltier system. For each sample, CD spectra were recorded at 220 nm as a function of temperature, from 25 to 100 °C. The sample was placed in a sealed cuvette to prevent water evaporation. In order to understand the change in protein conformation as a function of temperature, we studied the change in ellipticity at 220 nm. The 220 nm ellipticity in the spectrum of native lysozyme in buffer at 25 °C was assumed to correspond to 100 % folded protein. The ellipticity at 100

°C was assumed to correspond to the unfolded protein. The folded fraction was computed as:

$$\text{Fraction Folded } = \frac{A_{220} - A_u}{A_f - A_u}$$

In this formula, A_{220} is the absorbance of the protein at different temperatures between 25 and 100 °C, A_u is the absorbance of the unfolded protein at 100 °C, and A_f is the absorbance of the folded protein at 25 °C.

2.6. Fluorescence spectroscopy

A fluorescence assay was performed at 25 °C using an LS55 spectrophotometer (Perkin Elmer, Waltham, MA). The excitation wavelength was fixed at 280 nm for the overall fluorescence emission. The slit widths for excitation and emission were both set at 10 nm. The lysozyme concentration was 0.5 mg/mL, and each spectrum was the average of six spectra. Each sample spectrum was obtained by subtracting the blank (without lysozyme).

2.7. Lysozyme activity

Solutions containing 400 unit/mL of lysozyme in 10 mM phosphate buffer at pH 2 and 7 were treated with the DBD and the lytic activity of lysozyme was assessed using spectrophotometry. The principle is based on the phenomenon of cell wall lysis caused by the enzyme in *Micrococcus lysodeicticus* Gram-positive bacteria (Sigma-Aldrich). The lysozyme activity was determined by monitoring the decrease in turbidity of the bacterial suspension at 450 nm for 3 min.

2.8. Identification of oxidative modifications

Oxidative modifications were detected on the peptide level after digestion with trypsin followed by liquid chromatography – tandem mass spectrometry (LC-MS/MS), as described previously [37]. Briefly, RapiGest SF Surfactant (Waters) was added to a final concentration of 0.1% followed by incubation for 5 min at 100 °C. Samples were reduced (1 h at 55 °C) and alkylated (30 min in the dark) using 200 mM TCEP and 375 mM 2-iodoacetamide, respectively, before being precipitated with acetone overnight at -20 °C. The pellet was resuspended in 100 mM triethylammonium bicarbonate, and MS grade trypsin protease (Thermo Scientific) was added to a protease-protein ratio of 1:40 (w/w)

for digestion overnight at 37 °C. The digested sample was analysed on a nanoAcquity UPLC system (Waters) coupled to an LTQ ion trap mass spectrometer (Thermo Scientific) applying optimized settings for peptide separation and fragmentation, as described previously [37].

Peptide identification was performed by Proteome Discoverer (2.1 SP1) software (Thermo Scientific) by searching against the UniProt reference human database using Sequest and Mascot algorithm [38,39]. Search parameters were applied as follows: precursor mass tolerance 500 ppm, fragment mass tolerance 0.5 Da, and trypsin specificity allowing for up to two missed cleavages. Carbamidomethylation of cysteine was defined as fixed modification, and oxidations of the following residues were set as variable modifications: Methionine (Met), Tyrosine (Tyr), Aspartic acid (Asp), Phenylalanine (Phe), Histidine (His), Tryptophan (Trp), Asparagine (Asn), and Proline (Pro). The results were further filtered to only use highly confident peptides with a global FDR < 5% based on a target-decoy approach [40]. The list of first ranked oxidized peptides (see Table S1-S7 in supporting information) was checked manually to count the actual number of oxidation sites.

2.9. Molecular dynamics (MD) simulations

The MD simulations were performed in GROMACS 5.1.2 package [41] using the GROMOS54A7 force field [42]. The lysozyme structure was taken from the protein data bank (PDB 1DPX). The protein was solvated with water, described by the simple point charge (SPC) explicit solvent model [43]. Subsequently, the system was neutralized by Na^+ or Cl^- ions replacing the water molecules. The system was energy minimized with the steepest descent method. The NPT (i.e., at constant number of particles (N), pressure (P) and temperature (T)) equilibration was first carried out for 10 ns at 300 K and 1 bar by applying positional restraints (force constant of 1000 kJ mol^{-1} nm^{-2}) on the heavy atoms of the protein. This was done to keep the system as close as possible to its crystal structure. We employed V-rescale modified Berendsen thermostat with a time constant of 0.1 ps [44], Parrinello-Rahman barostat with a time constant of 2 ps [45], and isothermal compressibility of 4.5×10^{-5} bar^{-1} [46]. The cut-off radii of the van der Waals and Coulomb interactions were 1 nm. Additionally, the PME (particle mesh Ewald) summation was used to calculate the long-range electrostatic interactions [47], applying

long-range dispersion corrections for both energy and pressure. After the equilibration, we performed unrestrained (normal) MD simulations for another 400 ns, of which the last 10 ns was used to calculate the average values. In all simulations, a time step of 2 fs was used. Finally, we calculated the root mean square deviation (RMSD) of the backbone atoms, the root mean square fluctuations (RMSFs) of the protein residues and the solvent-accessible surface area (SASA), and we applied principle component analysis (PCA).

Besides simulating the native lysozyme structure in water, we also performed the same simulations for an oxidized form of lysozyme (oxidation product obtained from mass spectrometry). We modified the Trp28 and Tyr53 amino acids for lysozyme at pH 7 to 6-hydroxytryptophan and 3,4-dihydroxyphenylalaine, respectively. For lysozyme at pH 2, we modified both Phe34 and Phe38 to Tyrosine, and Tyr53 and Asn59 to 3,4-dihydroxyphenylalaine and 3-hydroxyasparagine, respectively, which are the most probable oxidized structures after plasma treatment based on literature [48]. For the oxidized amino acids, the GROMOS54A7 force field parameters were obtained from [49,50].

2.10. Cell culture
In this study, we have used two human melanoma (SK-MEL-2 and G361) and one normal keratinocyte (HACAT) cells. Human SK-MEL-2 were maintained in Minimum Essential Media (MEM; Welgene), while G361 and HACAT cells were maintained in Roswell Park Memorial Institute (RPMI-1640; Welgene). All media were supplemented with 10 % heat-inactivated fetal bovine serum (FBS) and 100 U/mL penicillin, 100 µg/mL streptomycin. Cell cultures were maintained at 37 °C, in a humidified 5 % CO_2 atmosphere.

2.11. Treatment of plasma treated and untreated lysozyme solutions for cell experiments
Lysozyme solutions were prepared at 1 mg/mL - 40 mg/mL concentrations in Phosphate Buffered Saline (PBS; Gibco) to determine direct effect of untreated lysozyme solutions on cancer and normal skin cells. Plasma-treated and untreated lysozyme solutions were prepared to analyze viability of cells. For this study, 1 mL lysozyme solution was directly exposed to DBD plasma discharge for 10 min at a distance of 5 mm in 6 well plate (SPL, Korea). Further, higher concentration of plasma-treated lysozyme (80 mg/mL) prepared

and serially diluted in plasma-treated and untreated buffer for comparison between plasma-treated lysozyme and serially diluted treated lysozyme in treated buffer.

2.12. Cell viability assays

The day before treatment, 40000 cells per well of SK-MEL-2, G361 melanoma and HACAT skin cells were seeded in a 24-well plate (SPL, Korea), and fresh medium was added to each well. After 24 h, media was removed and 200 μL of PBS (control), untreated lysozyme, and plasma-treated lysozyme solutions were added to each well for all three cell lines, and incubated for 30 min at 37 °C. Subsequently, 600 μL of fresh cell culture media were added to each well of all cell lines, and incubated further for 24 h at 37 °C. After 24 h, cells were incubated with Alamar Blue Cell Viability Reagent (Thermo Scientific, Korea) was added to each well. The cell viability was measured with a plate reader using fluorescence at 540 nm (ex.)/600 nm (em.). To check the time-dependent effect of untreated lysozyme and plasma-treated lysozyme solutions, cells were incubated until 96 h post-treatment and cell viability was recorded. Three biological replicates were used for the cell viability assay. A GraphPad Prism 9 inbuild statistical analysis software was employed to investigate the statistically significant changes (*$p < 0.05$, ** $p < 0.01$, ***$p < 0.001$) between control and treated samples.

2.13. Apoptosis confirmation studies

To determine the fraction of apoptotic cells following 24 h post-incubation, the cells were collected in polystyrene round-bottom test tubes (Greiner) and centrifuged for 5 min at 1500 rpm and the supernatant was discarded. Subsequently, 200 μL Annexin-V buffer solution (1/100 AnnexinV-FITC (BD Bioscience) in AnnV binding buffer was added to each sample. After 20 min incubation, the cells were immediately measured using FACSVerse (BD, biosciences) and analyzed with FACS Suite software. Three biological replicates were performed per condition.

Caspase levels in treated cells were observed using Caspase-Glo 9 and Caspase-Glo 3/7 Assay kits (Promega, Korea) as per manufacturer's instructions. For morphological analysis, nucleus condensation was observed in cells exposed with untreated and plasma-treated lysozyme solutions using Hoechst fluorescent stain solution

(Sigma Aldrich, Korea). Stained cells were photographed using confocal microscope (Olympus confocal live-cell imaging system). Cells were counted manually to visualize fragmented nuclei using three independent fields (1000 cells/field).

3. Results

3.1. Effect of plasma-induced oxidation on conformation and thermal stability of lysozyme

Lysozyme has 129 amino acid residues that contain three tyrosine (Tyr), six tryptophan (Trp), and four disulfide bonds [51]. Figures 1a and 1b display the negative bands in the range from 200 to 250 nm. The signal intensity at 208 nm was higher than at 222 nm, which is characteristic of an α + β protein [52]. We observed negative peaks at ≈ 208 and ≈ 222 nm in both acidic and neutral pH spectra. This is consistent with literature that lysozyme maintains its native content of secondary structure at different pH solutions [53,54]. At pH 2, after 5 min plasma treatment, we observed a decrease in the negative band at ≈ 208 nm, but no change at ≈ 222 nm, in Figure 1a. However, a broad negative peak around 230 nm appeared. This abnormality at 230 nm may be partly due to exciton coupling between the aromatic residues during denaturation of the protein [55,56]. Furthermore, prolonged plasma treatment for 10 and 20 min results in a lower peak intensity at ≈ 208 and 222 nm, but a higher intensity at 230 nm at pH 2 (Figure 1a). These changes in peaks may be due to the denaturation of lysozyme. On the other hand, the spectra after 5 and 10 min of plasma treatment at pH 7 show a slightly decreased peak at ≈ 208 and 222 nm, but no change in the peak at 230 nm, which shows the lysozyme structure was modified but not denatured (Figure 1b). At a prolonged treatment for 20 min, a red shift at ≈ 208 nm appeared, but no change in the peak at 230 nm, which indicates that the lysozyme structure is not denatured even at a high plasma dose at pH 7.
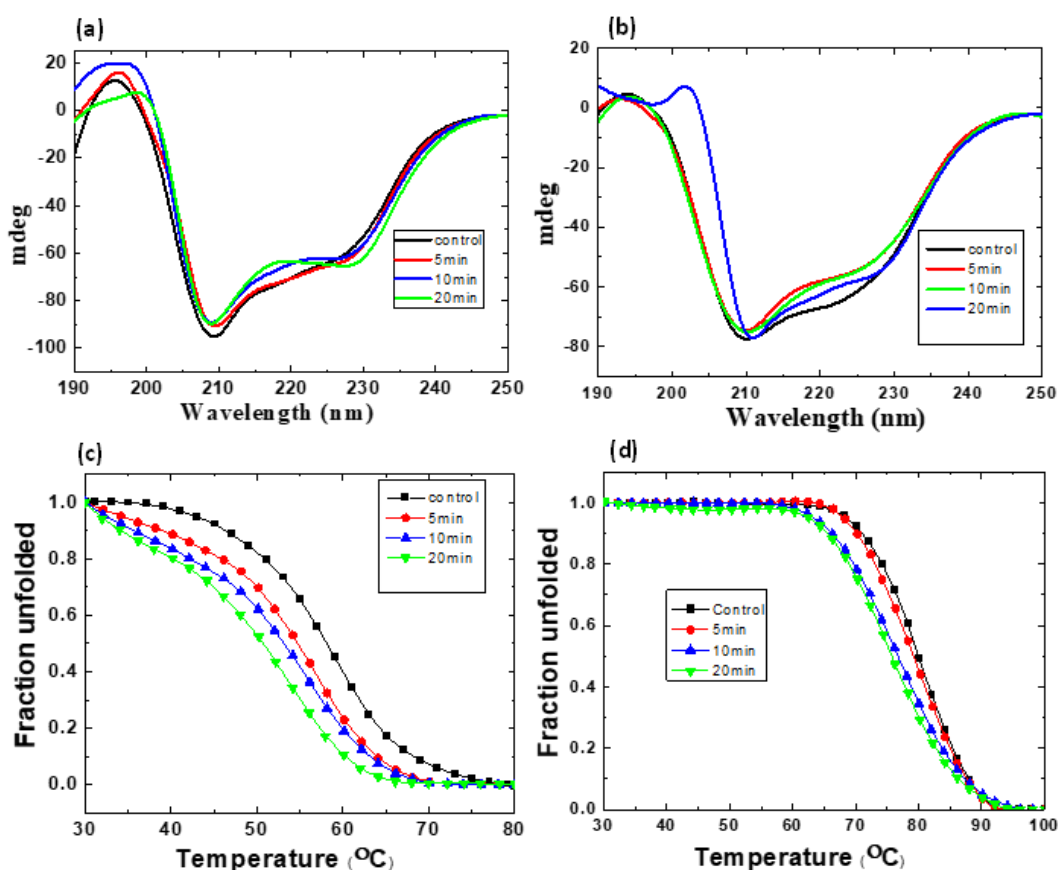
Figure 1. Secondary structure analysis of lysozyme at pH 2 (a) and pH 7 (b). Thermal analysis of lysozyme at pH 2 (c), and pH 7 (d). CD results are presented as average value of six replicates. Ellipticity reported in millidegrees (mdeg).

We used CD spectroscopy to determine the change in melting temperature (T_m) of lysozyme upon plasma treatment. The melting temperature was analyzed at 220 nm, before and after plasma treatment, as shown in Figures 1c and 1d, and Table 1. In previous reports, the T_m of lysozyme at pH 2 was 54.8 ± 0.2°C [57] and in water it was 77.19 ± 0.01 °C [58], which are quite similar to our obtained values. We observed a difference of 22 °C in the T_m when lysozyme was at pH 2 and 7. The T_m of lysozyme at pH 2 decreased by 4 °C after 5 min of plasma treatment, whereas plasma did not induce significant changes in the T_m of lysozyme at pH 7. Longer plasma treatments of 20 min reduced the T_m of lysozyme at pH 2 by 8 °C and by 5 °C in lysozyme at pH 7. The results suggest that prolonged plasma treatments affect the thermal stability of lysozyme independently of the pH, while short plasma treatment significantly influences the lysozyme melting point at acidic pH.

10

Table 1. Change in melting temperature of lysozyme at different pH after DBD treatment

Samples	Melting temperature (°C) [1]
pH 7	
Control	80.0 ±0.1
5 min DBD treatment	79.0 ±0.1
10 min DBD treatment	76.0 ±0.7
20 min DBD treatment	75.0 ±0.7
pH 2	
Control	58.0 ±0.2
5 min DBD treatment	54.0 ±0.7
10 min DBD treatment	53.0 ±0.1
20 min DBD treatment	50.0 ±0.8

[1] Results are presented as means ± SEM (n = 6).

Based on the CD analysis, we can conclude that structural deformation after plasma treatment was more substantial at pH 2 than at pH 7. Additionally, the change in T_m of plasma-treated lysozyme (pL) strongly depends on the pH.

3.2. Tryptophan quenching analysis after plasma treatment

The lysozyme's intrinsic fluorescence spectrum at pH 2 and 7 before and after plasma treatment is shown in Figures 2a and 2b. Lysozyme consists of 3 Tyrosine (Tyr) residues and 6 Tryptophan (Trp) residues. The intrinsic fluorescence in lysozyme is due to Trp, as it presents high intrinsic anisotropy. Trp is about one order of magnitude more fluorescent than Tyr, and two orders of magnitude more fluorescent than Phe [59]. Before plasma treatment, lysozyme at pH 2 and 7 exhibited a maximum emission spectrum at approx. 344 nm, and the intensity gradually decreased upon longer plasma treatment time (Figure 2a and b). At pH 2, we saw quenching of the maximum emission peak, but no change in the peak shift was observed. In contrast, at pH 7 we observed a red shift in the maximum emission for longer plasma treatment compared to the control. The maximum emission peak observed for 5, 10, and 20 min was 346, 354, and 354 nm, respectively. Hence, no change in maximum emission wavelength was found for 10 and 20 min of plasma

treatment, as shown in Figure 2b. This might be because no further change in the environment of Trp occurred for treatments of 10 and 20 min at pH 7.
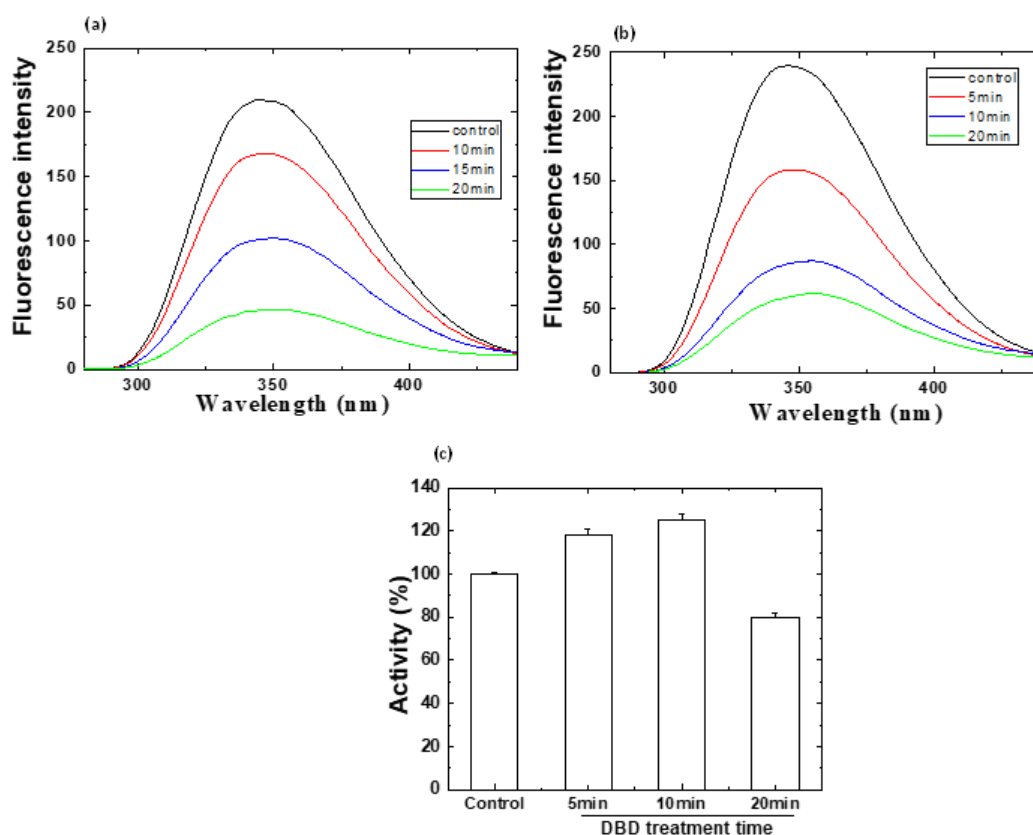

Figure 2. Fluorescence analysis of lysozyme at pH 2 (a) and pH 7 (b). Lysozyme antibacterial activity (c). Fluorescence results are presented as average value of six replicates. Lysozyme lytic activity results are presented as means ± SD, n=3.

In summary, quenching of the lysozyme peak was noted after plasma treatment during fluorescence analysis for lysozyme solutions at both pH 2 and 7, but a red shift with quenching was observed only for lysozyme solutions at pH 7, suggesting a modification of the Trp group and modified Trp exposure to the solvent. At pH 2, Trp was probably also modified, but not exposed to the solvent.

3.3. Lysozyme activity before and after plasma treatment

To evaluate whether the structural changes in lysozyme can affect its enzymatic activity, we performed an activity test (lytic activity) after plasma treatment for lysozyme at pH 2 and 7. The lysozyme assay assesses the ability of lysozyme to degrade the bacterial cell wall of *Micrococcus lysodeikticus*. The change in the percentage of lysozyme activity was

measured at pH 2 and 7. We observed that untreated lysozyme at pH 2 presented an enzymatic activity of less than 10 % compared to control (data not shown), which was consistent with previous results [60]. After plasma treatment, a complete loss in activity was observed (not shown).

pL at pH 7 increased its enzymatic activity to 118 % and 125 % after 5 and 10 min of plasma treatment, respectively. Longer plasma treatments (20 min) decreased this value to 80 % of the untreated (control) sample (Figure 2c). Enhancing the lysozyme activity by modification or by using different solvents is of great interest [61–63]. Cegielska-Radziejewska et al. showed that chemically modified lysozyme had higher antibacterial activity than monomeric lysozyme, being more effective against Gram-negative than to Gram-positive bacteria [64]. At physiological pH, a net positive and negative charge is found on lysozyme and the bacterial cell wall, respectively, which plays an essential role during the hydrolysis [65,66]. In addition, the replacement of Trp62 with Tyr62 residue in hen egg-white lysozyme enhanced its antibacterial activity [61]. Therefore, it is possible that the improved antibacterial activity of pL is due to modifications of specific amino acids in the protein chain. To know which amino acids were modified after plasma treatment, we performed mass spectrometry analysis.

3.4. Mass spectrometry analysis of lysozyme before and after plasma treatment

To localize plasma-induced oxidations, we performed LC-MS/MS on trypsin-digested lysozyme. For this purpose, lysozyme was treated with DBD plasma at both pH 2 and 7 for various time points before being digested into peptides. This bottom-up fashion not only allows for protein identification by allocating peptides based on their detected mass and fragments, but also to localize site-specific modifications in proteins by applying appropriate search algorithms [38,39]. As we were solely interested in plasma-induced oxidations, we screened for oxidative modifications in eight amino acids (Met, Tyr, Asp, Phe, His, Trp, Asn, and Pro) during the analysis. Table 2 summarizes identified oxidations in control and pL at both pH 2 and 7, for 10 min plasma treatment. This time point was chosen based on the obtained results of lysozyme activity at pH 7 (see Figure 2 above). Untreated lysozyme shows no oxidations at both pH, whereas after plasma treatment for 10 min at pH 2 and 7, four and two oxidations were identified, respectively.

Table 2. Overview of identified oxidations after plasma treatment. Number of plasma-induced oxidations and type of amino acid affected in control and pL at pH 2 and 7. Eight amino acids (Met, Tyr, Asp, Phe, His, Trp, Asn, and Pro) were chosen as variable oxidation sites for the analysis with Mascot and Sequest.

Amino acids	Control (pH 2)	Plasma treatment (pH 2)	Control (pH 7)	Plasma treatment (pH 7)
Asparagine	0	1	0	0
Phenylalanine	0	2	0	0
Tryptophan	0	0	0	1
Tyrosine	0	1	0	1
Total	0	4	0	2

Figure 3 highlights the plasma-induced oxidations on the structure of lysozyme (1dpx.pdb). Although Tyr53 exhibited an oxidation after plasma treatment at both pH, this residue has not shown reactivity in literature after iodination of lysozyme, which was explained by its localization in the pocket formed by the cross-β structure (Ala42-Gly54) and a hydrogen bond-stabilized coil (Cys64-Pro70) [67]. Trp28, the second amino acid that is oxidized after plasma treatment at pH 7, is also buried in the inside of the 3D structure of the protein. In literature, Trp28 reaction with 2-hydroxy-5-nitrobenyzl bromide was reported [68], but not with ozone [69], N-bromosuccinimide [70], and iodine [71]. Hence, plasma has proven to also reach chemically inaccessible residues.

At pH 2, however, plasma-induced oxidations showed a different pattern. Beside Tyr53, three other amino acids displayed oxidation after plasma treatment, e.g., Phe34, Phe38, and Asn59 (Figure 3). Most notably, these residues are in close spatial proximity, surrounded by several amino acids with charged side chains. Under acidic conditions, these amino acids can be considered protonated, which might lead to repelling forces in this region and consequently favour these residues for oxidation via ˙OH. Beside the 3D structure, it is also conceivable that the proteins' primary structure, i.e., neighbouring amino acids and their charges, have an influence on plasma and its potential in oxidizing proteins. Since plasma treatment led to a different oxidation pattern depending on the pH,

we performed MD simulations to investigate the impact of these oxidative modifications on the structure of lysozyme (see further).
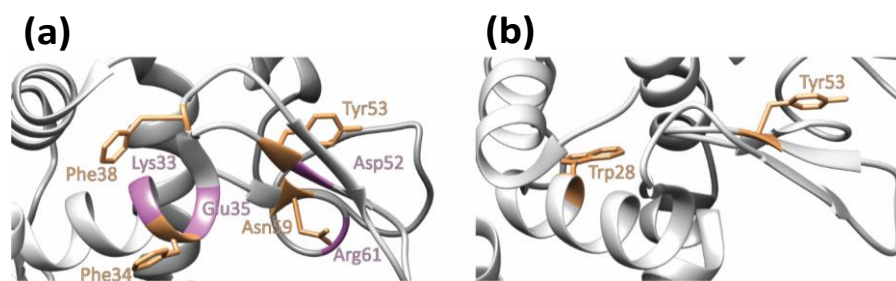

Figure 3: Oxidative modifications of lysozyme after plasma treatment. In total, four (Phe34, Phe38, Tyr53, and Asn59) and two (Trp28 and Tyr53) amino acid residues exhibit oxidation after plasma treatment at pH 2 (a) and pH 7 (b), respectively. Amino acids with charged side chains in the surrounding of identified modifications at pH 2 are labelled in purple. PDB: 1dpx.

3.5. Mass spectrometry analysis of lysozyme peptides before and after plasma treatment
To know whether plasma could modify other amino acids besides the ones mentioned above, independently of their position in the 3D structure of lysozyme, we trypsin-digested the lysozyme samples and then treated the resulting peptides with plasma at different pH. Moreover, with this experiment we can also show whether the pH of the solution influences plasma and its tendency to induce oxidations. As shown in Table 3, the fraction of PSM of oxidized peptides was higher at pH 2, independent of whether the treatment was performed on the globular protein or on peptides. These results support our above conclusion that plasma-induced oxidation of lysozyme is more prominent in acidic than in neutral solution, which is in agreement with a previous report by Chou et al [72]. The authors noticed a faster oxidation of Met[696] in the presence of tertiary-butyl hydroperoxide (TBHP) in 10 mM phosphate buffer at pH 2 compared to pH 7 [72]. Another study shows an increased oxidation rate in cells by changing from neutral to acidic pH [73].

Table 3: Overview of peptide spectrum matches w/o oxidations. As can be seen, the fraction of PSM of oxidized peptides is higher at pH 2, independent of whether the treatment was performed on the globular protein or on peptides only. This finding points to a higher prevalence of plasma-induced oxidations at pH 2 than at pH 7.

		#PSM total	#PSM oxidations
Protein	pH 2	8	4
treatment	pH 7	13	2
Peptide	pH 2	27	13
treatment	pH 7	23	7

3.6. MD simulation of native and oxidized lysozymes

Based on the MS analysis and the previously reported oxidation state of amino acids by plasma [48], we performed MD simulations to calculate the RMSD, RMSF, SASA, and to perform PCA analysis for both native and oxidized lysozyme proteins, to evaluate the effect of plasma treatment. As observed in Table 2, several amino acids were modified after plasma treatment. For oxidized lysozyme at pH 2, we changed Tyr53, Asn59, Phe34, and Phe38, while at pH 7, we modified Trp28 and Tyr53, based on the MS information. Asn, Phe, Trp, and Tyr were modified to 3-hydroxyasparagine, tyrosine, 6-hydroxytryptophan, and 3,4-dihydroxyphenylalanine, respectively, based on reference [48]. We performed the MD simulation for the native and oxidized lysozymes. Figure 4a shows the RMSD of the backbone atoms of both native and oxidized lysozyme in water for 400 ns simulation. The calculated average RMSD values were 0.22 ± 0.01, 0.32 ± 0.01, and 0.22 ± 0.02 nm for the native, oxidized acidic lysozyme (at pH 2) and oxidized neutral lysozyme (at pH 7), respectively. This indicates that the flexibility of oxidized acidic lysozyme was higher than for native and oxidized neutral lysozyme.

Figure 4b illustrates the RMSF as a function of residue number. The residues between 32-44, 65-74, and 116-124 faced a higher fluctuation for oxidized acidic lysozyme than for native and oxidized neutral lysozyme. For oxidized neutral lysozyme, the residues between 18-22, 100-105, and 127-129 show high fluctuation compared to native and oxidized acidic lysozyme. Among all the studied systems, the maximum RMSF of 0.48 nm^2 was observed for oxidized acidic lysozyme for the residues between 65-74.

Figure 4c shows the SASA results, which give information about the lysozyme's surface area that is accessible to water. The average SASA values of the native, oxidized acidic lysozyme and oxidized neutral lysozyme were 72 ± 2, 73 ± 1, and 72 ± 1 nm^2,

respectively. The SASA results show a slight increase for the oxidized lysozymes compared to the control lysozyme, although there was no significant difference between native and plasma-treated samples. Finally, Figure 4d shows the PCA results, which provide information about the total phase space that both native and oxidized lysozyme can occupy. The sum of eigenvalue was 1.8 nm^2 for the native lysozyme, while it was 2.0 nm^2 for the oxidized lysozymes at both pH. PCA analysis revealed that the structure of lysozyme becomes more flexible after oxidation of the amino acids.
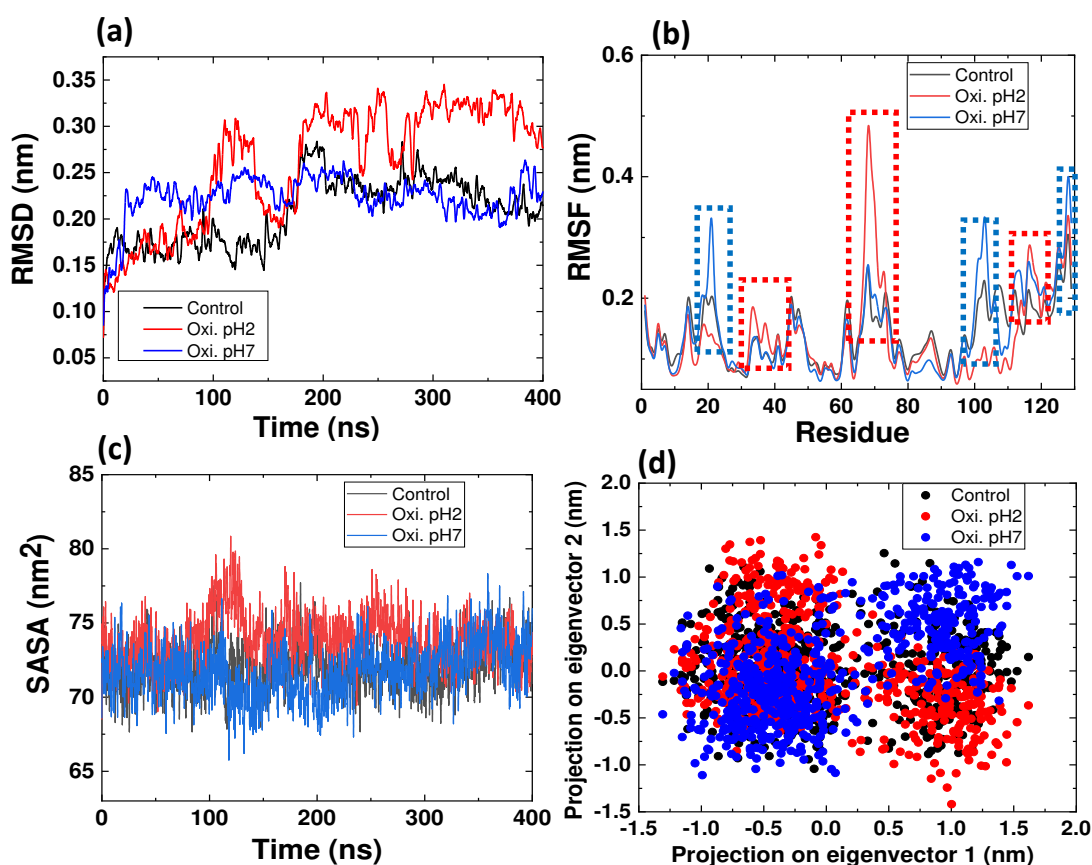

Figure 4. MD simulation of lysozyme for native (control), oxidized acidic lysozyme (Oxi. pH2) and oxidized neutral lysozyme (Oxi. pH7). (a) RMSD, (b) RMSF, (c) SASA and (d) PCA analysis.

3.7. Cancer cell killing effect of the plasma-treated lysozyme solutions

To evaluate the cancer cell killing potential of the pL at pH 7, we studied its effect on the viability of SK-MEL2, G361, and HACAT cell lines. To avoid the negative effect of acidic pH on cell viability, we only used a lysozyme solution at pH 7. For this investigation, we added different concentrations of lysozyme solutions to cancer (SK-

MEL-2 and G361) and normal skin (HACAT) cells. We observed no significant change in cancer cell viability with untreated lysozyme addition at all studied concentrations, regardless of the cell line tested, as shown in Figures 5a, 5c, and 6.

Subsequently, SK-MEL-2 and G361 cancer cells were treated at different pL concentrations, as shown in Figures 5b and 5d. Our data show that pL has a cytotoxic effect against SK-MEL2 cancer cells at 10-40 mg/mL, while 1 mg/mL pL has no effect. For the G361 cancer cells, pL showed cytotoxic effect only at 20 and 40 mg/mL. Notably, pL40 kills approximately 60 % of SK-MEL2 cells, while only 40 % of G361 cells. This difference in pL activity could depend on the mode of action of the cancer cell lines' target drug and characteristics. When we tested the effect of pL on normal HACAT cells, it showed around 15-20 % cell death only at higher concentrations (40 and 20 mg/mL). Figure S1 shows the cell viability of the two cancer cell lines and the normal cell line, as a function of incubation time. The time-dependent study shows that pL has a limited effect on the viability of HACAT cells after different treatments (pL40 treatment decreased the cell viability to approx. 25 %). On the other hand, a reduction in cell viability was observed for SK-MEL2 cells upon increasing incubation time with pL10-pL40 (approx. 60 % cells are killed after 96 h incubation with pL20 and pL40 treatments), while significant cell death for G361 cells was only observed with pL40 (approx. 40 % cells are killed after 96 h incubation) (Figure S1). These results show that G361 cancer cells exhibit more resistance towards the pL treatment than SK-MEL2 cells, and that pL40 treatment was more toxic towards cancer cells than normal cells.

Furthermore, we investigated the combination effect of plasma-treated buffer (PTB) and pL on the SK-MEL-2 and G361 cells. For this experiment, 80 mg/mL pL was serially diluted in PTB and untreated buffer (PBS) up to a concentration of 1 mg/mL. The addition of plasma-treated or untreated buffer hampered the pL cytotoxic activity. A small cell viability reduction in both cancer cell lines was observed after the dilution (Figures 5c, 5d, 5g, and 5h).
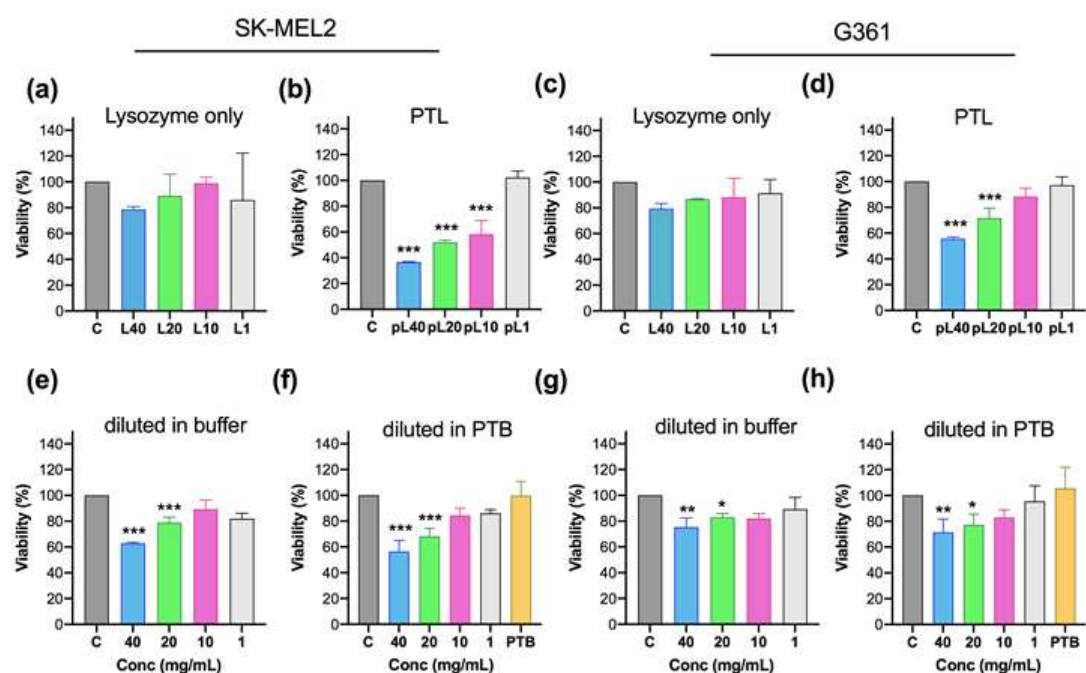
Figure 5. Viability assay using plasma-treated and untreated lysozyme solutions at pH 7, for SK-MEL2 (a-d) and G361 (e-f) cancer cells. Cells were exposed to untreated lysozyme (L) at different concentrations (40 to 1 mg/mL) (a,e); to plasma-treated lysozyme (pL) directly prepared (b,f); or by serial dilution in untreated buffer (c, g), or in plasma-treated buffer (PTB) (d,h). C = Untreated control. Results are presented as mean ± SEM (n = 3). Statistically significant differences are indicated as * $p < 0.05$, ** $p < 0.01$, and *** $p < 0.001$ between untreated lysozyme and corresponding treated groups. Significance was determined using the student's t-test.

A similar effect was also observed in HACAT cells when treated with pL diluted in PTB and untreated buffer (Figure 6). The cancer cell death effect of pL dilution in PTB is not significantly different from that of pL dilution in untreated buffer (PBS) (Figure S2). Additionally, PTB alone does not show a cytotoxic effect on both normal and cancer cell lines (Figures 5f, 5h and 6d). Therefore, we conclude that the cell death in this study is mainly due to the pL, with only a small contribution from the RONS present in the pL solutions.
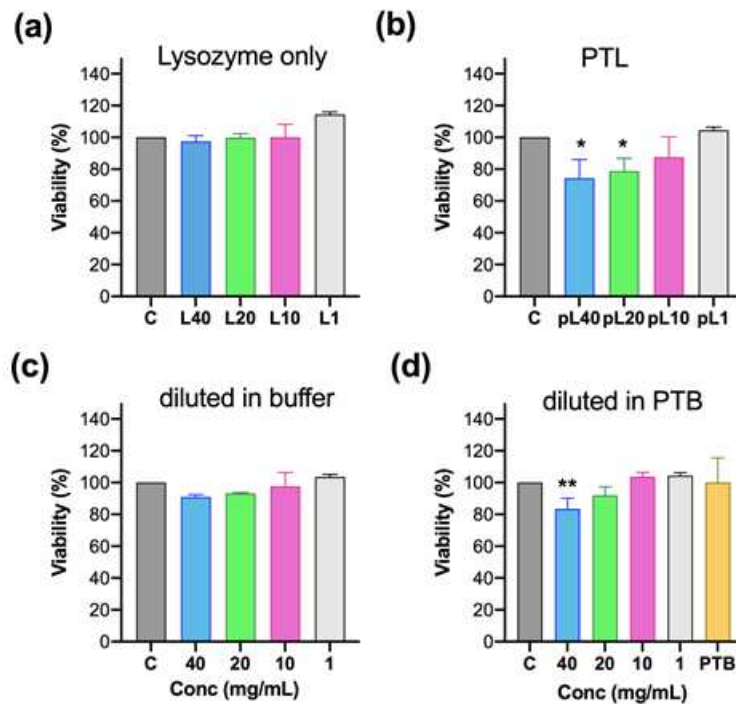
Figure 6. Viability assay using plasma-treated and untreated lysozyme solutions at pH 7, for HACAT cells. Cells were exposed to untreated lysozyme (L) at different concentrations (40 to 1 mg/mL) (a); to plasma-treated lysozyme (pL) directly prepared (b); or by serial dilution in untreated buffer (c), or in plasma-treated buffer (PTB) (d). C = Untreated control. Results are presented as means ± SEM (n = 3). Statistically significant differences are indicated as * $p < 0.05$, ** $p < 0.01$, and *** $p < 0.001$ between untreated lysozyme and corresponding treated groups. Significance was determined using the student's t-test.

Next, we evaluated whether our plasma-treated lysozyme (pL) could induce cell death by apoptosis in the skin cancer cells and normal cells. For this purpose, we applied fluorescent Annexin-V to SK-MEL2, G361 and HACAT cells for the detection of early apoptotic cells by flow cytometry after treatment. The cells were harvested 24h after incubation with the individual treatments and stained for the required analysis. Interestingly, the pL solutions induced cellular apoptosis at concentrations of 20 and 40 mg/mL. Indeed, as shown in Figure 7, the pL solutions result in a larger number of apoptotic cells in the cancer cells than in the normal cells, at concentrations of 20 and 40 mg/mL.
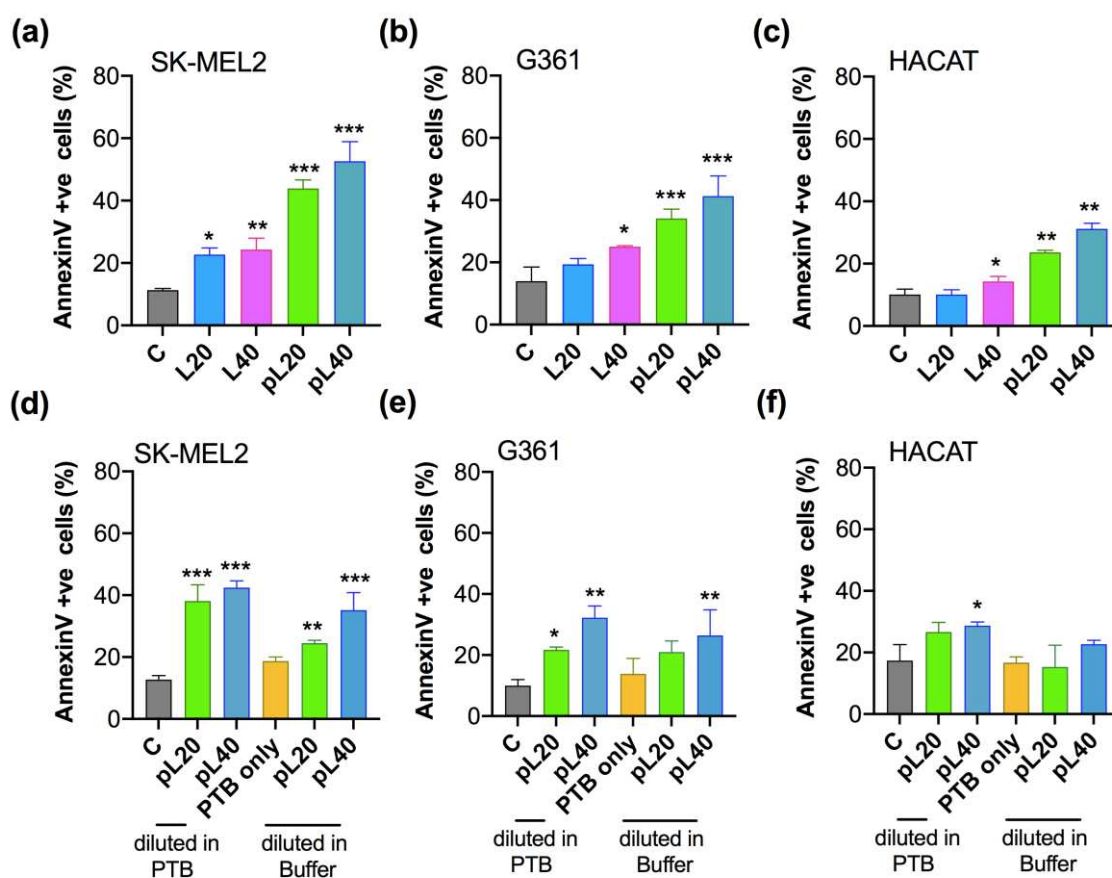
Figure 7. Apoptosis assays using plasma-treated and untreated lysozyme solutions at pH 7, for SK-MEL2, G361 and HACAT cells. (a-c) The cells were exposed to untreated lysozyme (L) and plasma-treated lysozyme (pL), both at concentrations of 20 and 40 mg/mL. (d-f) The cells were exposed to plasma-treated lysozyme (pL) by serial dilution in plasma-treated buffer (PTB) or untreated buffer. C = Untreated control. Results are presented as means ± SEM (n = 3). Statistically significant differences are indicated as * $p < 0.05$, ** $p < 0.01$, and *** $p < 0.001$ between untreated lysozyme and corresponding treated groups. Significance was determined using the student's t-test.

Additionally, as observed earlier, the addition of plasma-treated or untreated buffer significantly impeded the pL20 and pL40 effect on cellular apoptosis (Figures 7d-7f). The treatment with pL20 and pL40 results in approx. 45 % and 58 % apoptosis in SK-MEL2 cells, respectively (Figure 7a). This reduces to approx. 40 % after dilution with PTB (Figure 7d). Moreover, the fraction of apoptotic cells decreased to approx. 25 % and 40 % when pL20 and pL40 are diluted with untreated buffer. A similar trend is observed for

G361 and HACAT cells. However, the reduction in the number of apoptosis cells was higher when pL20 was diluted with buffer than PTB. Hence, it is possible that RONS in PTB play a role in improving apoptosis in comparison with untreated buffer. It is important to note that the number of apoptotic cells decreases after dilution in PTB or buffer; hence, we believe that plasma-modified lysozyme is the main player inducing apoptosis in all cell lines.

We also verified the caspase activity in the normal and cancer cell lines after treatment. Interestingly, we observed that pL increased caspase-3/7 and caspase-9 activity in both cancer cell lines, but caspase-9 was less pronounced than caspase-3/7 (Figures 8a and 8b). However, pL did not significantly affect the HACAT cells, as shown in Figure 8c. To clarify further, we stained pL-treated SK-MEL-2 with Hoechst and observed enhanced nuclear condensation and fragmented apoptotic bodies. Nuclear fragmentation was more pronounced in the pL-treated cancer cells than in the normal cells (Figure 8d, 8e). These results indicate that pL has the potential to stimulate cancer cell death via apoptosis induction.
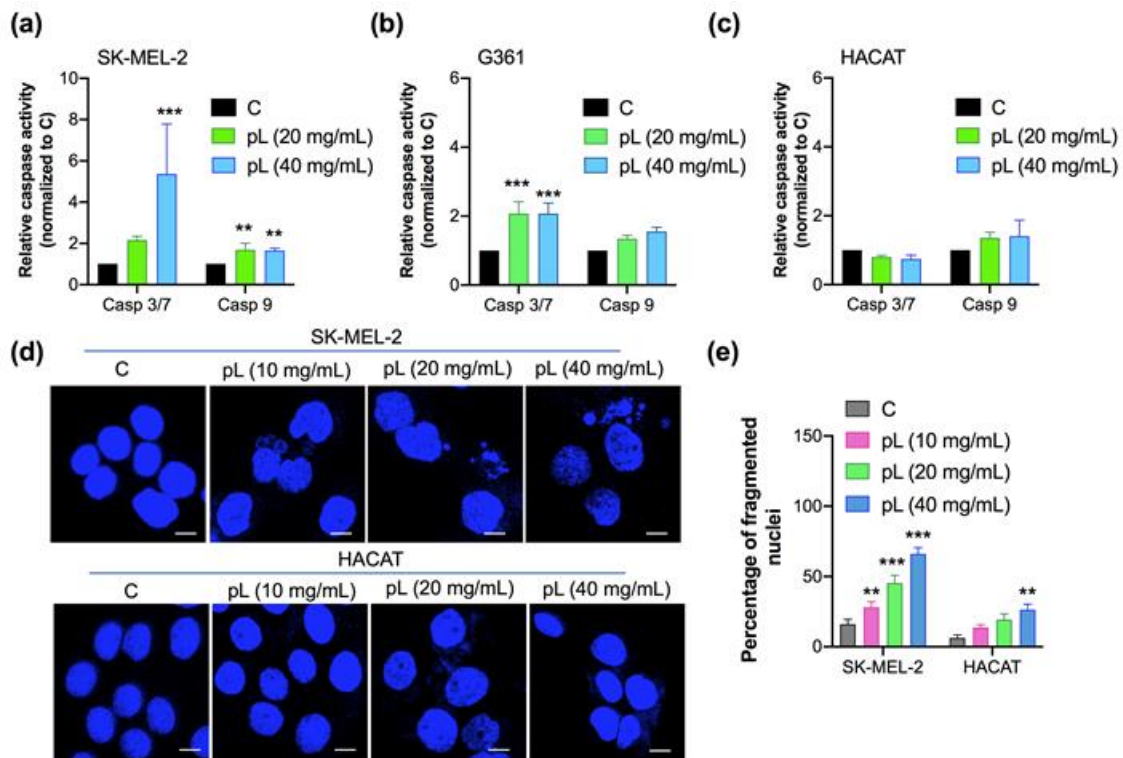
Figure 8. Plasma-treated lysozyme (pL) induces apoptosis in cancer cells. (a-c) Caspase-3/7 and Caspase-9 assay in SK-MEL-2, G361 cancer and HACAT normal skin cells, treated with pL at concentrations of 20 and 40 mg/mL. (d) Fluorescence images of cellular nucleus stained with Hoechst stain in SK-MEL-2 cancer and HACAT normal skin cells to verify nuclear condensation and morphology. (e) Representative graph, showing the quantification of fragmented nuclei, which are shown in panel d. Results are presented as means $\pm$ SEM (n = 3). Scale = 20 μm. The statistically significant differences are indicated as ** $p < 0.01$, and *** $p < 0.001$ between untreated lysozyme and corresponding treated groups. Significance was determined using the student's t-test.

4. Discussion

Secondary structure and tertiary structure analysis of lysozyme at different pH and with varying doses of plasma were recorded by CD and fluorescence spectroscopy. The changes in lysozyme's secondary structure were not significant for lower plasma treatment time at pH 7, but the changes were significant at pH 2. The quenching in the Trp group was observed after plasma treatment at both pH, but the quenching with red shift was observed for pL at pH 7. It may be due to the modification of Trp or the Trp environment, which results in Trp exposure to the solvent, leading to the red shift with quenching [74]. The fluorescence quenching was observed in our previous studies with different protein systems after plasma treatment [28,32]. The lysozyme activity increased after 5 and 10 min plasma treatment, but later decreased for prolonged plasma treatment. It was reported that lysozyme shows anticancer and antibacterial behavior even if there was a decrease in lysozyme lytic activity [22,75]. Vilcacundo et al. noticed that the lysozyme lytic activity was lost after thermal and chemical treatments, but the antibacterial effect of denatured lysozyme increased for Gram-negative bacteria by destroying the cell wall [76]. Mahanta et al. showed a decreased lysozyme lytic activity by self-assembled nanostructures but an improved cancer cell killing effect against breast cancer cells compared to native lysozyme [22].

Furthermore, MS analysis showed 56 % amino acids oxidized at pH 2, and 15 % at pH 7 after 10 min plasma treatment. Oxidation of amino acids is stronger in acidic than in neutral conditions. This is supported by previous work [77–79], and might be due to the stability and production of ˙OH radicals by the Fenton and Haber-Weiss chemistry or

through peroxynitrite, ONOO⁻ favored at acidic pH. Sellak et al. reported that the radicals produced by the Fenton reaction can deactivate the lysozyme if Fe is bound to the lysozyme [80], and this was also supported by Tompkins et al. [81]. Additionally, it was mentioned that amino acids of iron-bound lysozyme might be oxidized, but they keep their activity [80]. Our MD simulations also support our experimental results that the oxidized acidic lysozyme structure becomes more unstable than when oxidized at pH 7. PCA analysis revealed that oxidized acidic lysozyme covered a larger region of phase space along PC1 and PC2 compared to the native and oxidized neutral lysozyme.

It was earlier reported that lysozyme shows cancer cell killing effect at high concentration (1-400 mg/mL, depending on the cell line), but this high concentration also kills healthy cells [7,19]. Therefore, we wanted to evaluate the cell death by lysozyme on different cell lines. 40 mg/mL lysozyme treatment does not have significant effect on both normal and cancer cells, although 40 mg/mL pL kills both normal (approx.10-20%) and cancer cells (approx. 40-60 %, depends upon cell type). At lower concentration of 10 mg/mL, pL does not have toxic effect on normal cells, but it kills 40% of SK-MEL2 cancer cells, whereas it fails to kill G361 cancer cells. The pL cytotoxic effect decreases during the dilution in untreated buffer or in PTB. Additionally, PTB alone did not show a significant cytotoxic effect on both normal and cancer cell lines (see Figures 5, 6 and 7). In our previous work using the kINPen® IND plasma jet, we shown that PTB treated for 9 min had 1400 μM H_2O_2, which evoked a cytotoxic effect in cancer cells [82]. In contrast, the DBD device used in this study generates 25 μM H_2O_2 for 5 min treatment [28]. We believe that the absence of a cytotoxic effect in the present study could be explained by the use pulsed DBD with lower energy than the previously employed kINPen® IND plasma jet.

Hence, it is possible that there is no combination effect of pL with PTB. The small decrease in cytotoxicity of pL upon dilution might be due to renaturation of lysozyme from the plasma-modified structure that decreases the cytotoxic effect, although we believe that modification of the amino acids keeps the cytotoxic property of pL. We observed that plasma-induced amino acids oxidation in lysozyme retains up to 1 month at 4 °C, it might hold for long until lysozyme degraded, but we have not studied that in present work. Earlier studies also reported the refolding of lysozyme upon dilution

[83,84] that might reverse the plasma-induced structural modification of lysozyme, which results in decreased cytotoxic effect .

Additionally, increased caspase-3/7 and caspase-9 activities was observed in both cancer cell lines after pL treatment. Hence, pL have the potential to stimulate cancer cell death via apoptosis induction. Further, dilution with PTB or buffer is less effective than direct plasma exposure to specific protein concentrations. Therefore, we suggest that direct exposure to biomolecules at a specific concentration will be more effective than further diluting it in PTB or media for future studies.

It is known that the administration of lysozyme to tumor cells results in cell death by the creation of azurophilic granules in the cytoplasm [85]. FITC-conjugated lysozyme was found on the cell surface, as well as in the intracellular organelles [21]. This shows that lysozyme can enter the cancer cells and form granules, resulting in damage of the cell membrane for cell cultures. Another group reported that the treatment with nanostructured lysozyme damaged the cytoplasmic membrane, resulting in an increased ROS production that triggered cell death. Based on our results, we especulate that the cell death observed in cancer cells is mainly due to the plasma-treated lysozyme damage to the cell membrane and not plasma-generated RONS in the solution, although the mechanism still not clear. In our system, direct effect of plasma-generated RONS on the cell death is limited (Figures 5-7). We believe that short- and long-lived RONS produced by plasma in pL solutions will mainly interact with lysozyme and modify its structure. The remaining long-lived RONS in pL will be significantly less after their interaction with lysozyme, which will interact with the biomolecules in the cells. Our experiments with PTB alone (Figures 5-7) reveal a small amount of toxicity towards both normal and cancer cells (not statistically significant). These findings support our assumption that in our treatment, plasma produced RONS mainly used to modify lysozyme structure.

5. Conclusion

In this study, we investigated the plasma-induced structural deformation of lysozyme in acidic and neutral pH. The plasma-induced oxidation was stronger in acidic pH than in neutral pH. The plasma-induced structural modification resulted in significant cytotoxic effect towards cancer cells, but not towards healthy cells. However, more investigations

are required, e.g., to standardize the treatment conditions, before this could be brought into *in-vivo* treatments.

Conflicts of Interest: The authors declare no conflict of interest.

References

1. Vasan, N.; Baselga, J.; Hyman, D.M. A view on drug resistance in cancer. *Nature* **2019**, *575*, 299–309, doi:10.1038/s41586-019-1730-1.

2. Torres, W.; Lameda, V.; Olivar, L.C.; Navarro, C.; Fuenmayor, J.; Pérez, A.; Mindiola, A.; Rojas, M.; Martínez, M.S.; Velasco, M.; et al. Bacteria in cancer therapy: beyond immunostimulation. *J. Cancer Metastasis Treat.* **2018**, *4*, 4, doi:10.20517/2394-4722.2017.49.

3. Kramer, M.G.; Masner, M.; Ferreira, F.A.; Hoffman, R.M. Bacterial Therapy of Cancer: Promises, Limitations, and Insights for Future Directions. *Front. Microbiol.* **2018**, *9*, 1–9, doi:10.3389/fmicb.2018.00016.

4. Zahaf, N.; Schmidt, G. Bacterial Toxins for Cancer Therapy. *Toxins (Basel).* **2017**, *9*, 236, doi:10.3390/toxins9080236.

5. Saruc, M.; Standop, S.; Standop, J.; Nozawa, F.; Itami, A.; Pandey, K.K.; Batra, S.K.; Gonzalez, N.J.; Guesry, P.; Pour, P.M. Pancreatic enzyme extract improves survival in murine pancreatic cancer. *Pancreas* **2004**, *28*, 401–12.

6. Zheng, K.; Lu, M.; Liu, Y.; Chen, Q.; Taccardi, N.; Hüser, N.; Boccaccini, A.R. Monodispersed lysozyme-functionalized bioactive glass nanoparticles with antibacterial and anticancer activities. *Biomed. Mater.* **2016**, *11*, 035012, doi:10.1088/1748-6041/11/3/035012.

7. Sava, G.; Benetti, A.; Ceschia, V.; Pacor, S. Lysozyme and cancer: Role of exogenous lysozyme as anticancer agent (review). *Anticancer Res.* 1989, *9*, 583–591.

8. Osserman, E.F. Postulated relationships between lysozyme and immunoglobulins as mediators of macrophage and plasma cell functions. *Adv. Pathobiol.* 1976, *4*, 98–105.

9. Gordon, S.; Todd, J.; Cohn, Z.A. In vitro synthesis and secretion of lysozyme by

mononuclear phagocytes. *J. Exp. Med.* **1974**, doi:10.1084/jem.139.5.1228.

10. Mason, D.Y.; Taylor, C.R. The distribution of muramidase (lysozyme) in human tissues. *J. Clin. Pathol.* **1975**, doi:10.1136/jcp.28.2.124.

11. Osserman, E.F.; Lawlor, D.P. Serum and urinary lysozyme (muramidase) in monocytic and monomyelocytic leukemia. *J. Exp. Med.* **1966**, doi:10.1084/jem.124.5.921.

12. PELLEGRINI, A.; THOMAS, U.; BRAMAZ, N.; KLAUSER, S.; HUNZIKER, P.; VON FELLENBERG, R. Identification and isolation of a bactericidal domain in chicken egg white lysozyme. *J. Appl. Microbiol.* **1997**, *82*, 372–378, doi:10.1046/j.1365-2672.1997.00372.x.

13. Yabe, N.; Komiya, K.; Takezono, T.; Matsui, H. Lysozyme as a regulator of interleukin-2-activated lymphocyte proliferation. *Vitr. Cell. Dev. Biol. - Anim. J. Soc. Vitr. Biol.* **1993**, *29*, 795–806, doi:10.1007/BF02634347.

14. LeMarbre, P.; Rinehart, J.; Kay, N.; Vesella, R.; Jacob, H. Lysozyme enhances monocyte-mediated tumoricidal activity: a potential amplifying mechanism of tumor killing. *Blood* **1981**, *58*, 994–999, doi:10.1182/blood.V58.5.994.994.

15. Deckx, R.J.; Vantrappen, G.R.; Parein, M.M. Localization of lysozyme activity in a Paneth cell granule fraction. *BBA - Enzymol.* **1967**, doi:10.1016/0005-2744(67)90136-2.

16. TAHARA, E.; ITO, H.; SHIMAMOTO, F.; IWAMOTO, T.; NAKAGAMI, K.; NIIMOTO, H. Lysozyme in human gastric carcinoma: a retrospective immunohistochemical study. *Histopathology* **1982**, *6*, 409–421, doi:10.1111/j.1365-2559.1982.tb02738.x.

17. Wittekind, C.; Wachner, R.; Henke, W.; Kleist, S. Localization of CEA, HCG, Lysozyme, alpha-1-antitrypsin, and alpha-1-antichymotrypsin in gastric cancer and prognosis. *Virchows Arch. A Pathol. Anat. Histopathol.* **1986**, *409*, 715–724, doi:10.1007/BF00713436.

18. *Lysozyme*; ELLIOTT F. OSSERMAN, R.E.C. and S.B., Ed.; Elsevier, 1974; ISBN 9780125289504.

19. Guo, T.K.; Zhao, X.H.; Xie, X.D.; Chen, Z.H.; Zhou, C.S.; Wei, L.L.; Zhang, H. The anti-proliferative effects of recombinant human lysozyme on human gastric cancer cells. *J. Int. Med. Res.* **2007**, *35*, 353–360, doi:10.1177/147323000703500310.

20. Murakami, F.; Sasaki, T.; Sugahara, T. Lysozyme stimulates immunoglobulin production by human-human hybridoma and human peripheral blood lymphocytes. *Cytotechnology* **1997**, *24*, 177–182, doi:10.1023/A:1007936629501.

21. Sugahara, T.; Murakami, F.; Yamada, Y.; Sasaki, T. The mode of actions of lysozyme as an immunoglobulin production stimulating factor. *Biochim. Biophys. Acta - Gen. Subj.* **2000**, *1475*, 27–34, doi:10.1016/S0304-4165(00)00041-6.

22. Mahanta, S.; Paul, S.; Srivastava, A.; Pastor, A.; Kundu, B.; Chaudhuri, T.K. Stable self-assembled nanostructured hen egg white lysozyme exhibits strong anti-proliferative activity against breast cancer cells. *Colloids Surfaces B Biointerfaces* **2015**, *130*, 237–245, doi:10.1016/j.colsurfb.2015.04.017.

23. Darby, J.F.; Atobe, M.; Firth, J.D.; Bond, P.; Davies, G.J.; O'Brien, P.; Hubbard, R.E. Increase of enzyme activity through specific covalent modification with fragments. *Chem. Sci.* **2017**, *8*, 7772–7779, doi:10.1039/C7SC01966A.

24. Korystova, A.F.; Kublik, L.N.; Levitman, M.K.; Samokhvalova, T. V.; Shaposhnikova, V. V.; Korystov, Y.N. Ionizing Radiation Enhances Activity of Angiotensin-Converting Enzyme in Rat Aorta. *Bull. Exp. Biol. Med.* **2018**, doi:10.1007/s10517-018-4133-7.

25. Souza, M.S.; Hansson, L.-A.; Hylander, S.; Modenutti, B.; Balseiro, E. Rapid Enzymatic Response to Compensate UV Radiation in Copepods. *PLoS One* **2012**, *7*, e32046, doi:10.1371/journal.pone.0032046.

26. Ke, Z.; Huang, Q. Inactivation and Heme Degradation of Horseradish Peroxidase Induced by Discharge Plasma. *Plasma Process. Polym.* **2013**, *10*, 731–739, doi:10.1002/ppap.201300035.

27. Attri, P.; Choi, E.H. Influence of Reactive Oxygen Species on the Enzyme Stability and Activity in the Presence of Ionic Liquids. *PLoS One* **2013**, *8*, e75096, doi:10.1371/journal.pone.0075096.

28. Attri, P.; Park, J.H.; De Backer, J.; Kim, M.; Yun, J.H.; Heo, Y.; Dewilde, S.; Shiratani, M.; Choi, E.H.; Lee, W.; et al. Structural modification of NADPH oxidase activator (Noxa 1) by oxidative stress: An experimental and computational study. *Int. J. Biol. Macromol.* **2020**, *163*, 2405–2414, doi:10.1016/j.ijbiomac.2020.09.120.

29. Attri, P.; Kumar, N.; Park, J.H.; Yadav, D.K.; Choi, S.; Uhm, H.S.; Kim, I.T.; Choi, E.H.; Lee, W. Influence of reactive species on the modification of biomolecules generated from the soft plasma. *Sci. Rep.* **2015**, *5*, 8221, doi:10.1038/srep08221.

30. Attri, P.; Kim, M.; Sarinont, T.; Ha Choi, E.; Seo, H.; Cho, A.E.; Koga, K.; Shiratani, M. The protective action of osmolytes on the deleterious effects of gamma rays and atmospheric pressure plasma on protein conformational changes. *Sci. Rep.* **2017**, *7*, 8698, doi:10.1038/s41598-017-08643-1.

31. Attri, P.; Sarinont, T.; Kim, M.; Amano, T.; Koga, K.; Cho, A.E.; Choi, E.H.; Shiratani, M. Influence of ionic liquid and ionic salt on protein against the reactive species generated using dielectric barrier discharge plasma. *Sci. Rep.* **2015**, *5*, 17781, doi:10.1038/srep17781.

32. Attri, P.; Han, J.; Choi, S.; Choi, E.H.; Bogaerts, A.; Lee, W. CAP modifies the structure of a model protein from thermophilic bacteria: mechanisms of CAP-mediated inactivation. *Sci. Rep.* **2018**, *8*, 10218, doi:10.1038/s41598-018-28600-w.

33. Attri, P.; Razzokov, J.; Yusupov, M.; Koga, K.; Shiratani, M.; Bogaerts, A. Influence of osmolytes and ionic liquids on the Bacteriorhodopsin structure in the absence and presence of oxidative stress: A combined experimental and computational study. *Int. J. Biol. Macromol.* **2020**, *148*, 657–665, doi:10.1016/j.ijbiomac.2020.01.179.

34. Lee, K.H.; Kim, H.J.; Woo, K.S.; Jo, C.; Kim, J.K.; Kim, S.H.; Park, H.Y.; Oh, S.K.; Kim, W.H. Evaluation of cold plasma treatments for improved microbial and physicochemical qualities of brown rice. *LWT - Food Sci. Technol.* **2016**, *73*, 442–447, doi:10.1016/j.lwt.2016.06.055.

35. Li, H.P.; Wang, L.Y.; Li, G.; Jin, L.H.; Le, P.S.; Zhao, H.X.; Xing, X.H.; Bao, C.Y. Manipulation of lipase activity by the helium radio-frequency, atmospheric-pressure glow discharge plasma jet. *Plasma Process. Polym.* **2011**, *8*, 224–229, doi:10.1002/ppap.201000035.

36. Choi, S.; Attri, P.; Lee, I.; Oh, J.; Yun, J.-H.; Park, J.H.; Choi, E.H.; Lee, W. Structural and functional analysis of lysozyme after treatment with dielectric barrier discharge plasma and atmospheric pressure plasma jet. *Sci. Rep.* **2017**, *7*, 1027, doi:10.1038/s41598-017-01030-w.

37. De Backer, J.; Razzokov, J.; Hammerschmid, D.; Mensch, C.; Hafideddine, Z.; Kumar, N.; van Raemdonck, G.; Yusupov, M.; Van Doorslaer, S.; Johannessen, C.; et al. The effect of reactive oxygen and nitrogen species on the structure of cytoglobin: A potential tumor suppressor. *Redox Biol.* **2018**, *19*, 1–10, doi:10.1016/j.redox.2018.07.019.

38. Eng, J.K.; McCormack, A.L.; Yates, J.R. An approach to correlate tandem mass spectral data of peptides with amino acid sequences in a protein database. *J. Am. Soc. Mass Spectrom.* **1994**, *5*, 976–989, doi:10.1016/1044-0305(94)80016-2.

39. Perkins, D.N.; Pappin, D.J.C.; Creasy, D.M.; Cottrell, J.S. Probability-based protein identification by searching sequence databases using mass spectrometry data. In Proceedings of the Electrophoresis; Electrophoresis, 1999; Vol. 20, pp. 3551–3567.

40. Elias, J.E.; Gygi, S.P. Target-decoy search strategy for mass spectrometry-based proteomics. *Methods Mol. Biol.* **2010**, *604*, 55–71, doi:10.1007/978-1-60761-444-9_5.

41. M.J. Abraham, D. van der Spoel, E. Lindahl, B. Hess, and the G.; development team No Title. *GROMACS User Man. version 5.1.2* **2016**.

42. Schmid, N.; Eichenberger, A.P.; Choutko, A.; Riniker, S.; Winger, M.; Mark, A.E.; van Gunsteren, W.F. Definition and testing of the GROMOS force-field versions 54A7 and 54B7. *Eur. Biophys. J.* **2011**, *40*, 843–856, doi:10.1007/s00249-011-0700-9.

43. Berendsen, H.J.C.; Postma, J.P.M.; van Gunsteren, W.F.; Hermans, J. Interaction Models for Water in Relation to Protein Hydration. In; 1981; pp. 331–342.

44. Bussi, G.; Donadio, D.; Parrinello, M. Canonical sampling through velocity

rescaling. *J. Chem. Phys.* **2007**, *126*, 014101, doi:10.1063/1.2408420.

45.   Parrinello, M.; Rahman, A. Polymorphic transitions in single crystals: A new molecular dynamics method. *J. Appl. Phys.* **1981**, *52*, 7182–7190, doi:10.1063/1.328693.

46.   Berendsen, H.J.C.; Postma, J.P.M.; van Gunsteren, W.F.; DiNola, A.; Haak, J.R. Molecular dynamics with coupling to an external bath. *J. Chem. Phys.* **1984**, *81*, 3684–3690, doi:10.1063/1.448118.

47.   Darden, T.; York, D.; Pedersen, L. Particle mesh Ewald: An N ·log(N) method for Ewald sums in large systems. *J. Chem. Phys.* **1993**, *98*, 10089–10092, doi:10.1063/1.464397.

48.   Takai, E.; Kitamura, T.; Kuwabara, J.; Ikawa, S.; Yoshizawa, S.; Shiraki, K.; Kawasaki, H.; Arakawa, R.; Kitano, K. Chemical modification of amino acids by atmospheric-pressure cold plasma in aqueous solution. *J. Phys. D. Appl. Phys.* **2014**, *47*, 285403, doi:10.1088/0022-3727/47/28/285403.

49.   Margreitter, C.; Petrov, D.; Zagrovic, B. Vienna-PTM web server: a toolkit for MD simulations of protein post-translational modifications. *Nucleic Acids Res.* **2013**, *41*, W422–W426, doi:10.1093/nar/gkt416.

50.   Margreitter, C.; Reif, M.M.; Oostenbrink, C. Update on phosphate and charged post-translationally modified amino acid parameters in the GROMOS force field. *J. Comput. Chem.* **2017**, doi:10.1002/jcc.24733.

51.   Imoto, T.; Forster, L.S.; Rupley, J.A.; Tanaka, F. Fluorescence of lysozyme: emissions from tryptophan residues 62 and 108 and energy migration. *Proc. Natl. Acad. Sci. U. S. A.* **1972**, doi:10.1073/pnas.69.5.1151.

52.   *Circular Dichroism and the Conformational Analysis of Biomolecules*; Fasman, G.D., Ed.; Springer US: Boston, MA, 1996; ISBN 978-1-4419-3249-5.

53.   Polverino de Laureto, P.; Frare, E.; Gottardo, R.; van Dael, H.; Fontana, A. Partly folded states of members of the lysozyme/lactalbumin superfamily: A comparative study by circular dichroism spectroscopy and limited proteolysis. *Protein Sci.* **2009**, *11*, 2932–2946, doi:10.1110/ps.0205802.

54.   Rzeźnicka, I.I.; Pandey, R.; Schleeger, M.; Bonn, M.; Weidner, T. Formation of Lysozyme Oligomers at Model Cell Membranes Monitored with Sum Frequency Generation Spectroscopy. *Langmuir* **2014**, *30*, 7736–7744, doi:10.1021/la5010227.

55.   Matsuo, K.; Sakurada, Y.; Yonehara, R.; Kataoka, M.; Gekko, K. Secondary-Structure Analysis of Denatured Proteins by Vacuum-Ultraviolet Circular Dichroism Spectroscopy. *Biophys. J.* **2007**, *92*, 4088–4096, doi:10.1529/biophysj.106.103515.

56.   Sreerama, N.; Woody, R.W. Computation and Analysis of Protein Circular Dichroism Spectra. *Methods Enzymol.* **2004**, doi:10.1016/S0076-6879(04)83013-1.

57.   Arnaudov, L.N.; de Vries, R. Thermally Induced Fibrillar Aggregation of Hen Egg White Lysozyme. *Biophys. J.* **2005**, *88*, 515–526, doi:10.1529/biophysj.104.048819.

58.   Kamiyama, T.; Liu, H.L.; Kimura, T. Preferential solvation of lysozyme by dimethyl sulfoxide in binary solutions of water and dimethyl sulfoxide. In Proceedings of the Journal of Thermal Analysis and Calorimetry; 2009.

59.   Agro', A.F. Intrinsic fluorescence of a protein devoid of tyrosine and tryptophan: Horse hepatocuprein. *FEBS Lett.* **1974**, *39*, 164–166, doi:10.1016/0014-5793(74)80042-6.

60.   Kato, A.; Tanimoto, S.; Muraki, Y.; Kobayashi, K.; Kumagai, I. Structural and Functional Properties of Hen Egg-white Lysozyme Deamidated by Protein Engineering. *Biosci. Biotechnol. Biochem.* **1992**, doi:10.1271/bbb.56.1424.

61.   KUMAGAI, I.; KOJIMA, S.; TAMAKI, E.; MIURA, K. Conversion of Trp 62 of Hen Egg-White Lysozyme to Tyr by Site-Directed Mutagenesis. *J. Biochem.* **1987**, *102*, 733–740, doi:10.1093/oxfordjournals.jbchem.a122111.

62.   Kumagai, I.; Miura, K. ichiro Enhanced bacteriolytic activity of hen egg-white lysozyme due to conversion of trp62 to other aromatic amino acid residues. *J. Biochem.* **1989**, *105*, 946–948, doi:10.1093/oxfordjournals.jbchem.a122784.

63.   Wang, S.-C.; Lee, C.T. Enhanced Enzymatic Activity through Photoreversible Conformational Changes †. *Biochemistry* **2007**, *46*, 14557–14566, doi:10.1021/bi701073d.

64.   Cegielska-Radziejewska, R.; Lesnierowski, G.; Kijowski, J. Antibacterial activity of hen egg white lysozyme modified by thermochemical technique. *Eur. Food Res. Technol.* **2009**, *228*, 841–845, doi:10.1007/s00217-008-0997-5.

65.   RICHARDS, P.G.; WALTON, D.J.; HEPTINSTALL, J. The effects of tyrosine nitration on the structure and function of hen egg-white lysozyme. *Biochem. J.* **1996**, *315*, 473–479, doi:10.1042/bj3150473.

66.   Tanford, C.; Wagner, M.L. Hydrogen Ion Equilibria of Lysozyme. *J. Am. Chem. Soc.* **1954**, doi:10.1021/ja01641a076.

67.   Hayashi, K.; Shimoda, T.; Imoto, T.; Funatsu, M. Iodination of Lysozyme II. Reactivity and Position of Tyrosine Residues*. *J. Biochem.* **1968**, *64*, 365–370, doi:10.1093/oxfordjournals.jbchem.a128903.

68.   Barman, T.E. Reactivities of the tryptophan residues of α-lactalbumin and lysozyme to 2-hydroxy-5-nitrobenzyl bromide. *J. Mol. Biol.* **1970**, *52*, 391–394, doi:10.1016/0022-2836(70)90039-2.

69.   Jollès, P. Relationship between chemical structure and biological activity of hen egg-white lysozyme and lysozymes of different species. *Proc. R. Soc. London. Ser. B. Biol. Sci.* **1967**, *167*, 350–364, doi:10.1098/rspb.1967.0033.

70.   Hayashi, K.; Imoto, T.; Funatsu, G.; Funatsu, M. The position of the active tryptophan residue in lysozyme. *J. Biochem.* **1965**, *58*, 227–235,

doi:10.1093/oxfordjournals.jbchem.a128190.

71. Blake, C.C. A crystallographic study of the oxidation of lysozyme by iodine. *Proc. R. Soc. London. Ser. B. Biol. Sci.* **1967**, doi:10.1098/rspb.1967.0041.

72. Chou, D.K.; Krishnamurthy, R.; Manning, M.C.; Randolph, T.W.; Carpenter, J.F. Effects of solution conditions on methionine oxidation in albinterferon alfa-2b and the role of oxidation in its conformation and aggregation. *J. Pharm. Sci.* **2013**, *102*, 660–673, doi:10.1002/jps.23401.

73. Rego, A.C.; Duarte, E.P.; Oliveira, C.R. Oxidative stress in acidic conditions increases the production of inositol phosphates in chick retinal cells in culture. *Free Radic. Biol. Med.* **1996**, *20*, 175–187, doi:10.1016/0891-5849(95)02029-2.

74. Lakowicz, J.R.; Weber, G. Quenching of Protein Fluorescence by Oxygen. Detection of Structural Fluctuations in Proteins on the Nanosecond Time Scale. *Biochemistry* **1973**, doi:10.1021/bi00745a021.

75. Yang, T.; Leśnierowski, G. Changes in selected physicochemical properties of lysozyme modified with a new method using microwave field and oxidation. *PLoS One* **2019**, *14*, e0213021, doi:10.1371/journal.pone.0213021.

76. Vilcacundo, R.; Méndez, P.; Reyes, W.; Romero, H.; Pinto, A.; Carrillo, W. Antibacterial activity of hen egg white lysozyme denatured by thermal and chemical treatments. *Sci. Pharm.* **2018**, doi:10.3390/scipharm86040048.

77. Baker, M.S.; Gebicki, J.M. The effect of pH on the conversion of superoxide to hydroxyl free radicals. *Arch. Biochem. Biophys.* **1984**, doi:10.1016/0003-9861(84)90348-5.

78. Crow, J.P.; Spruell, C.; Chen, J.; Gunn, C.; Ischiropoulos, H.; Tsai, M.; Smith, C.D.; Radi, R.; Koppenol, W.H.; Beckman, J.S. On the pH-dependent yield of hydroxyl radical products from peroxynitrite. *Free Radic. Biol. Med.* **1994**, doi:10.1016/0891-5849(94)90034-5.

79. Shu, Z.; Jung, M.; Beger, H.-G.; Marzinzig, M.; Han, F.; Butzer, U.; Bruckner, U.B.; Nussler, A.K. pH-dependent changes of nitric oxide, peroxynitrite, and reactive oxygen species in hepatocellular damage. *Am. J. Physiol. Liver Physiol.* **1997**, *273*, G1118–G1126, doi:10.1152/ajpgi.1997.273.5.G1118.

80. Sellak, H.; Franzini, E.; Hakim, J.; Pasquier, C. Mechanism of lysozyme inactivation and degradation by iron. *Arch. Biochem. Biophys.* **1992**, *299*, 172–178, doi:10.1016/0003-9861(92)90259-Y.

81. Tompkins, G.R.; O'Neill, M.M.; Cafarella, T.G.; Germaine, G.R. Inhibition of bactericidal and bacteriolytic activities of poly-D-lysine and lysozyme by chitotriose and ferric ion. *Infect. Immun.* **1991**, *59*, 655–664, doi:10.1128/iai.59.2.655-664.1991.

82. Van Boxem, W.; Van der Paal, J.; Gorbanev, Y.; Vanuytsel, S.; Smits, E.; Dewilde, S.; Bogaerts, A. Anti-cancer capacity of plasma-treated PBS: effect of chemical composition on cancer cell cytotoxicity. *Sci. Rep.* **2017**, *7*, 16478,

doi:10.1038/s41598-017-16758-8.

83.   Gao, Y.G.; Guan, Y.X.; Yao, S.J.; Cho, M.G. Refolding of lysozyme at high concentration in batch and fed-batch operation. *Korean J. Chem. Eng.* **2002**, *19*, 871–875, doi:10.1007/BF02706982.

84.   Gao, Y.G.; Guan, Y.X.; Yao, S.J.; Cho, M.G. Lysozyme refolding at high concentration by dilution and size-exclusion chromatography. *J. Zhejiang Univ. Sci.* **2003**, *4*, 136–141, doi:10.1631/jzus.2003.0136.

85.   CALLERIO, C. Appearance of Granules in the Cytoplasm of Tumour-Cell Cultures in Contact with Lysozyme. *Nature* **1959**, *184*, 202–203, doi:10.1038/184202a0.